This is a preprint, the final version is subject to change, of the American Mineralogist (MSA)
Cite as Authors (Year) Title. American Mineralogist, in press.
(DOI will not work until issue is live.) DOI: http://dx.doi.org/10.2138/am-2015-4911

REVISION 1

Mössbauer spectroscopic study of natural eosphorite, [(Mn, Fe)$AlPO_4(OH)_2H_2O$]

Antoine Van Alboom[1,2], Valdirene Gonzaga de Resende[1], Geraldo Magela da Costa[3] and Eddy De Grave[1*]

[1]Department of Physics and Astronomy, University of Ghent, B-9000 Gent, Belgium

[2]Department of Industrial Technology and Construction, University of Ghent, B-9000 Gent, Belgium

[3]Chemistry Department, Federal University of Ouro Preto, 35400-000, Ouro Preto (MG), Brazil

* E-mail: eddy.degrave@UGent.be

Abstract

A ^{57}Fe Mössbauer spectroscopic study of natural eosphorite, (Mn, Fe^{2+})$AlPO_4(OH)_2H_2O$, is reported. The Mössbauer spectra were collected at temperatures between 295 K and 4.2 K. At temperatures exceeding 30 K, the Mössbauer spectra consist of a somewhat broadened quadrupole doublet with a splitting of 1.73 mm/s at 295 K. From the spectrum recorded at 250 K in an external magnetic field of 60 kOe, it is derived that the sign of the principal component of the electric field gradient (EFG) is negative and that the EFG's asymmetry parameter is large (~0.5). From these findings, it is concluded that the octahedral coordination of the ferrous cations exhibits in first order a trigonal compression with a further lowering from axial symmetry due to an additional distortion. The spectrum collected at 4.2 K shows the existence of magnetic ordering. It was analysed in terms of the full hyperfine interaction Hamiltonian, yielding a magnetic hyperfine field value of 146 kOe and EFG characteristics that are fully in line with those obtained from the external-field spectrum. In the temperature range from 10 to 30 K, the spectra indicate the occurrence of relaxation effects. They could be satisfactorily described in terms of the Blume-Tjon (BT) model for electronic relaxation, assuming a superposition of a slow- and a fast-relaxation component. The observed temperature dependence of the isomer shift is adequately described by the Debye model for the lattice vibrations. The characteristic Mössbauer temperature was found as (360 ± 20) K and the zero-Kelvin intrinsic isomer shift as (1.480 ± 0.005) mm/s. The variation of the quadrupole splitting with temperature is explained by the thermal population of the Fe^{2+} electronic states within the T_{2g} orbital triplet, which is split by the trigonal crystal field in a singlet ground state and an upper doublet state, the latter being further split into two orbital singlets by an additional distortion. The energies of these latter excited states with respect to the ground state are calculated to be 280 ± 20 cm^{-1} and 970 ± 50 cm^{-1}, respectively, based on a point-charge calculation of the ^5D level scheme. This calculation confirms the sign of the V_{zz}

component of the electric field gradient being negative as it is determined from the external magnetic field measurement and from the magnetic spectrum acquired at 4.2 K. Iron phosphates are widely spread minerals in the Earth's crust and are expected to occur in soils and rocks on Mars as well. Mössbauer spectroscopy as complimentary source of information to the results of other analytical techniques, could therefore be useful to identify and characterize the environmental Fe-bearing phosphates.

Keywords: eosphorite, Mössbauer spectroscopy, hyperfine parameters, temperature variation

INTRODUCTION

Eosphorite, ideally $Mn^{2+}AlPO_4(OH)_2.H_2O$, has orthorhombic symmetry with space group *Bbam* (Hanson 1960, Huminicki and Hawthorne 2002). The structure is depicted in Figure 1 and consists of alternating chains of Mn octahedra and Al octahedra that run parallel to the *c*-axis. The strongly-distorted Mn octahedra share opposite O1-O2 edges, while the more regular Al octahedra share opposite O3 corners occupied by H_2O groups. The two types of chains are linked to each other by sharing their O4 corners, thus forming parallel sheets that are held together by P cations in a tetrahedral O4 coordination. Based on single-crystal X-ray diffraction, Hoyos et al. (1993) concluded that the two aforementioned O4 sites are both occupied by OH groups. However, a more recent structure refinement using neutron diffraction data for a single-crystal of eosphorite has revealed that only one of the O4 sites is occupied by OH, while the other is occupied by H_2O (Gatta et al. 2013). Thus, the structure can be considered as being composed of chains of $MnO_4(OH,H_2O)_2$ and $AlO_2(OH)_2(OH,H_20)_2$ octahedra. Eosphorite is isomorphous with childrenite, $FeAlPO_4(OH)_2.H_2O$, and the two mentioned minerals form the end members of a complete solid-solution series. It is generally accepted in the literature that only Fe^{2+} is present in the structure of iron-substituted eosphorite, $(Mn,Fe)AlPO_4(OH)_2.H_2O$, and that these Fe^{2+} cations are found in the Mn octahedra.

Mössbauer spectra (MS) at room temperature (RT) of a number of iron-substituted eosphorites with different Fe/Mn ratios have been presented by da Costa et al. (2005). These authors found a relatively narrow ferrous doublet with constant isomer shift δ_{Fe} of 1.25 mm/s and quadrupole splittings ΔE_Q in the range 1.70 to 1.74 mm/s. More recently, Dyar et al. (2014) in a compilation of Mössbauer data on a large variety of phosphate minerals reported for a childrenite-eosphorite solid solution with unspecified Fe/Mn ratio a single quadrupole doublet with δ_{Fe} = 1.25 mm/s and ΔE_Q = 1.66 mm/s. As far as could be traced by the present

authors, no further Mössbauer data on childrenite-eosphorite solid solutions are available in the literature. In the present contribution, MS acquired at many different temperatures in the range between 4.2 K and 295 K for an eosphorite sample (RO-02, Fe/Mn ratio of 0.60) studied earlier by da Costa et al. (2005) are presented and the temperature variations of the isomer shift and the quadrupole interaction are discussed.

EXPERIMENTAL

The specimen of natural eosphorite was characterized by X-ray diffraction and microprobe analysis. The unit-cell parameters were calculated as a = 10.429 Å, b = 13.474 Å and c = 6.925 Å. Chemical analysis revealed the presence of 17.8 wt % MnO and 10.5 wt % FeO in the sample.

MS were collected at selected temperatures between 4.2 K and 295 K using spectrometers operating in constant acceleration mode with triangular reference signal. ^{57}Co(Rh) sources were used. A spectrum was acquired at ~250 K in a longitudinal external magnetic field of 60 kOe to determine the sign of the principal component V_{ZZ} of the electric field gradient (EFG) and the EFG's asymmetry parameter η. The counts were accumulated in 1024 channels. Spectra were run until an off-resonance count rate of at least 10^6 per channel was reached. The spectrometers were calibrated by collecting the RT spectrum of a reference metallic-iron foil or a standard α-Fe_2O_3 powder, depending on the applied velocity range. Isomer shifts quoted hereafter are referenced with respect to α-Fe at 295 K.

SPECTRA ANALYSES AND RESULTS

A typical Mössbauer spectrum of the eosphorite sample is reproduced in Figure 2 (RT). It has been fitted with a Lorentzian-shaped quadrupole doublet (solid line in Fig. 2), yielding the isomer shift δ_{Fe} and quadrupole splitting ΔE_Q values that are characteristic of

105 Fe^{2+}, *i.e.*, 1.24 mm/s and 1.73 mm/s at 295 K, respectively. The relatively narrow line width,
106 i.e. $\Gamma = 0.33$ mm/s at RT, suggests that the Fe^{2+} cations are indeed substituting for Mn^{2+} at the
107 Mn octahedra only. The MS for all applied temperatures down to 40 K are similar. Adjusted
108 values of δ_{Fe} and ΔE_Q for selected temperatures are listed in Table 1. Consistently, no
109 indication of the presence of any Fe^{3+} was noticed. At the lower applied temperatures, a
110 slightly lower goodness-of-fit was reached using a model-independent distribution of
111 quadrupole splittings for the fittings (Vandenberghe et al. 1994), instead of using a single
112 quadrupole doublet. However, the values calculated for the maximum-probability quadrupole
113 splittings of the respective distributions were found to coincide, within experimental error
114 limits, with those of the quadrupole splittings adjusted by the single-doublet model.

115 It is well known that the quadrupole splitting ΔE_Q as observed in a doublet spectrum is
116 given by the relation (Ingalls 1964):

117 $$\Delta E_Q = \Delta E_{Q,zz}\sqrt{1+\frac{1}{3}\eta^2}\ , \qquad (1)$$

118 in which

119 $$\Delta E_{Q,zz} = \frac{1}{2}eQ|V_{zz}| \qquad (2)$$

120

121 In Equation 2, e represents the proton charge, Q is the nuclear quadrupole moment and V_{zz}
122 (often denoted as eq) is the principal component of the electric field gradient (EFG) tensor,
123 being positive or negative depending on the local symmetry experienced by the probe ^{57}Fe
124 nuclei. $\eta = \left|V_{xx} - V_{yy}\right| / V_{zz}$ is the asymmetry parameter, being zero for axial symmetry. The
125 quantities V_{ii} are the diagonal elements of the EFG tensor organized so that $V_{zz} > V_{xx} \geq V_{yy}$. In
126 general, information about η and the sign of V_{zz} can be obtained from MS recorded for the
127 sample being subjected to a strong external magnetic field H_{ext} at a temperature in the
128 paramagnetic regime. Such measurement was performed for the eosphorite powder at 250 K

in an applied longitudinal field of 60 kOe. That spectrum is reproduced in Figure 3, in which the solid line is the numerically adjusted line shape.

The analysis of the external-field spectrum was based on the diagonalization of the full nuclear interaction Hamiltonian taking into account the variable spatial direction of the external magnetic field as expressed by the azimuthal and zenithal angles φ and θ with respect to the local EFG-axes system (Van Alboom et al. 2011). A total of 72 equally-spaced values for φ in the range 0° to 355° were considered, while for each φ value the quantity cosθ was forced to vary between 1 and -1 in steps of 0.1. Further, it was taken into account that in a paramagnetic powder the external magnetic field induces an internal magnetic field as a consequence of magnetization effects arising from a partial or full orientation of the magnetic moments along the direction of the external magnetic field. This effect is experienced as a strong reduction of the external field. For a paramagnetic cation such as Fe^{2+}, this reduction is moreover usually anisotropic in the sense that the effective field experienced by the probe Fe nuclei depends on the orientation of the external magnetic field with respect to the EFG-axes. This anisotropic effect is modeled by introducing three reduction parameters H_{xx}, H_{yy} and H_{zz}, respectively. Depending on the electronic structure of Fe^{2+}, i.e. on the ^5D level scheme in the local crystal field, the magnitude of one or more of these H_{ii} reductions may be high, even exceeding the magnitude of the applied field itself (Varret 1976).

Numerous trial fits were attempted. Consistently, a negative sign for V_{zz} was obtained as was a high magnitude for the field-reduction parameter H_{zz}. Moreover, the spectrum was most adequately reproduced by additionally introducing in the model a distribution of values for H_{zz}. For the calculated line shape shown in Figure 3, the adjusted values for δ_{Fe} and ΔE_Q were 1.25 ± 0.02mm/s and 1.88 ± 0.03mm/s ($V_{zz} < 0$), respectively. They are not highly accurate (see Table 1), but in reasonable agreement with the values expected from the results derived from the zero-field quadrupole doublets in the vicinity of 250 K. The value of 0.45 ±

0.05 for the asymmetry parameter implies that the symmetry of the Mn octahedron is non-axial, which is conceivable considering the known variations in O-O interatomic distances for that octahedron (Hoyos et al. 1993, Gatta et al. 2013). Calculated values of the field reduction parameters are H_{xx} = -5 ± 1 kOe, H_{yy} = -9 ± 2 kOe and H_{zz} = -90 ± 5kOe.

At 4.2 K, the mineral eosphorite exhibits magnetic ordering (Fig. 4). The spectrum was analyzed by an iteration procedure that is similar to the one applied to fit the earlier external-field spectrum (Fig. 3) and that makes use of the diagonalization of the full hyperfine-interaction Hamiltonian to calculate the relevant energy levels and the transition probabilities between these levels for a random powder absorber (Hoy and Chandra 1967; Kündig 1967). The hyperfine parameters that have to be adjusted in this procedure are (*i*) the isomer shift δ_{Fe}, (*ii*) the principal component V_{zz} of the EFG, (*iii*) the asymmetry parameter η of the EFG, (*iv*) the strength H_{hf} of the magnetic hyperfine field, and (*v*) the zenithal and azimuthal angles of the hyperfine field in the EFG (*x*,*y*,*z*)-axes frame, Ω and Ψ, respectively. However, this fitting approach produced an adjusted line shape that was clearly showing slight but significant misfits. These misfits were likely the result of the constraint imposed on the fit by considering one single component with constant line width for all eight transitions and/or from the feature that one or more hyperfine parameters to some extent exhibit a distribution. In general, Fe^{2+} hyperfine parameters, in particular the hyperfine field, are indeed very sensitive to such features as structural imperfections, locally varying bonding properties and nearest-neighbor cation configurations or slight deviations from ideal stoichiometry. Therefore, in a next stage of the numerical interpretation of the spectral data, a model-independent distribution of the hyperfine field H_{hf} was programmed (Vandenberghe et al. 1994), allowing this field to take on 40 successive values in a step of 5 kOe. It was further imposed that all 40 elemental components possess equal values for the other hyperfine parameters, *viz.*, δ_{Fe}, V_{zz}, and η, and for the angles Ω and Ψ.

The as-such adjusted Mössbauer spectrum is plotted as a solid line in Figure 4. It is obvious that the agreement with the observed spectrum is satisfactory. The obtained values for δ_{Fe} and ΔE_Q (see Table 1) are in line with those observed for the paramagnetic MS and the derived sign of V_{zz} is in agreement with that concluded from the external-field spectrum at 250 K, *i.e.*, negative. Also the values of the asymmetry parameter η found at 4.2 K and at 250 K are consistent. Further, the maximum-probability hyperfine field was calculated to be 146 ± 5 kOe and the angles Ω and Ψ were iterated to be 80 ± 2° and 260 ± 50°, respectively.

In the intermediate temperature range between ~10 K and ~35 K, the shape of the spectra indicate the occurrence of electronic relaxation. Two example spectra are reproduced in Figure 5. At first, the relaxation effect is reflected in the appearance of an asymmetric doublet (see Fig. 5a). The asymmetry becomes more enhanced as the temperature is further lowered. At 10 K, the presence of a second spectral component showing magnetic hyperfine structure is evident (see Fig. 5b). The relaxation spectra of this eosphorite sample are remarkably very similar to the spectra observed earlier for a natural ankerite species with composition $(Ca_{1.1}Mg_{0.5}Fe_{0.3}Mn_{0.1})(CO_3)_2$ (De Grave 1986). As for this carbonate, the present relaxation spectra are only adequately described by a superposition of a fast- and a slow-relaxation component in terms of the relaxation model described by Blume and Tjon (1968). In the iteration procedure, the hyperfine field was fixed at the value calculated for the spectrum at 4.2 K, i.e. 146 kOe. The other hyperfine parameters δ, ΔE_Q and η were allowed to vary and also the relaxation times τ_s and τ_f; the relative spectral areas S_s and S_f of the slow- and fast-relaxing component, respectively, were adjustable parameters. The calculated overall line shapes and the respective sub-components are plotted as solid lines in Figure 5. The agreement with the experimental line shapes is quite reasonable. The adjusted values for δ, ΔE_Q and η are included in Table 1 and are in line with the results derived from the pure paramagnetic spectra. The relaxation times were calculated as $\tau_s = 1.0\times10^{-8}$ s and $\tau_f = 1.6\times10^{-}$

^{10} s at 10 K, and $\tau_s = 6.7\times10^{-9}$ s and $\tau_f = 2.0\times10^{-10}$ s at 19 K. The S_f/S_s area ratios were found to be 50:50 and 70:30 at 10 K and 19 K, respectively. Being beyond the scope of this spectroscopic mineralogical characterization of eosphorite, no further attention was paid to the physical nature and the origin of these relaxation phenomena.

DISCUSSION

The temperature dependence of the isomer shift δ (the subscript *Fe* is from here on omitted for the sake of clarity) is plotted in Figure 6. The data are interpreted on the basis of the expression: $\delta(T) = \delta_I + \delta_{SOD}$. The intrinsic isomer shift δ_I is determined by the *s*-electron density at the nucleus and in a first approximation exhibits a linear temperature variation: $\delta_I(T) = \delta_I(0) + \alpha.10^{-5}T$. This weak variation is a result of the thermal expansion of the t_{2g} and e_g wave functions of the iron probes (Perkins and Hazony 1972). In contrast, the second-order Doppler shift, δ_{SOD}, is strongly dependent on temperature, being related to the vibrational properties of the probe nuclei in the crystal structure. The Debye approximation for the lattice vibrational spectrum provides an adequate model for calculating δ_{SOD}. It contains one parameter, the so-called characteristic Mössbauer temperature, Θ_M, that is obtained by adjusting the theoretical expression for $\delta(T)$ to the experimental values. Details concerning the calculation of the $\delta(T)$ curve in terms of the Debye model, are given in De Grave and Van Alboom (1991) and Eeckhout and De Grave (2003a). The solid curve in Figure 6 represents the calculated temperature variation with $\Theta_M = 360 \pm 20$ K. This result is in line with a general tendency that Fe^{2+} Mössbauer temperatures are close to 400 K, while Fe^{3+} species commonly exhibit values close to or exceeding 500 K. The thermal coefficient α was adjusted

to a value of –6.5 mm/(sK), which is significantly higher than is found for triphylite, *i.e.*, -1.1 mm/(sK) (Van Alboom et al. 2011), but comparable with the result obtained for hedenbergite, *i.e.*, -4.5 mm/(sK) (Eeckhout and De Grave 2003b). However, it must be stressed that in general the parameter α is ill defined because of the extremely small misfit effects it corrects for and because of the strong interference with the parameter Θ_M in determining the goodness-of-fit of the calculated $\delta(T)$ curve. This is especially true when the temperature range of the experimental data does not extend to very high values.

The temperature variation of the quadrupole splitting ΔE_Q is depicted in Figure 7. In general, each V_{ii} (i = x, y, or z) in Equations 1 and 2 is composed of a valence term and a lattice term, *i.e.*:

$$V_{ii} = (1-R)V_{ii,val} + (1-\gamma_\infty)V_{ii,latt}, \quad (3)$$

R and γ_∞ being the Sternheimer shielding and anti-shielding factors, respectively (Sternheimer 1972). The valence term (indicated by subscript *val*) reflects the contribution of the non-spherical charge distribution of the 3*d*-"valence" electrons of the Fe^{2+} ion, while the lattice term (indicated by subscript *latt*) originates from the charge distribution of the neighboring ions in the crystalline lattice.

The valence contributions are determined by the Boltzmann occupation of the ^5D energy levels of the Fe^{2+} probe ion (see hereafter), which largely explains the temperature dependence of the quadrupole splitting. The ^5D orbital energy level scheme itself is determined by the effect of the crystal field caused by the surrounding ions of the Fe^{2+} probe in the high spin state. The primary effect of the crystal field is to lift the five-fold spatial degeneracy of the ^5D state. In the case of a cubic field, the five orbital levels are split in a higher orbital doublet (E_g) and a lower orbital triplet (T_{2g}). A trigonal compression of the crystallographic site, for example, further splits the lower triplet in a lower singlet and a higher doublet. An additional distortion of lower than trigonal symmetry of the Fe^{2+}

253 crystallographic site further lifts the orbital degeneracy of the ^5D orbital energy level scheme
254 fully, giving rise to five separate orbital levels. For completeness, it should be mentioned that
255 spin-orbit interaction lifts the five-fold spin degeneracy of each of these five orbital levels.
256 However, this effect can be neglected in a first approximation.

257 The ^5D level scheme is obtained by diagonalization the crystal field Hamiltonian H_{cf},
258 which is expressed in the equivalent operator notation (Hutchings 1964) as:

259
$$\hat{\mathrm{H}}_{cf} = \sum_{n=2,4} \theta_n < r^n > \sum_{m=0}^{n} \sum_{(t)} A_{nm}^{(t)} \hat{\mathrm{O}}_{nm}^{(t)} = \sum_{n=2,4} \sum_{m=0}^{n} \sum_{(t)} B_{nm}^{(t)} \hat{\mathrm{O}}_{nm}^{(t)} \quad (4)$$

260 From this equation, the position of the ^5D energy levels and the corresponding wave functions
261 are calculated. The operator $\hat{\mathrm{O}}_{nm}^{(t)}$ is the Stevens' equivalent representation of the related
262 tesseral harmonic. The factor θ_n is required for the proper transformation to that
263 representation. The summation over t reflects the summation over equivalent operators
264 related to the relevant sine and cosine tesseral harmonics. $A_{nm}^{(t)}$ and $B_{nm}^{(t)}$ are coefficients
265 depending on the charges and the relative coordinates of the ligands with respect to the Fe^{2+}
266 probe in its coordination. The quantities $< r^2 >$ and $< r^4 >$ appearing in Equation 4 are the
267 expectation values of r^2 and r^4, related to the radial part of the ^5D wave functions. To calculate
268 the matrix elements of the crystal field Hamiltonian, the ligands were assumed to be point
269 charges with relative positions based on the point symmetry of the Fe^{2+} site in eosphorite
270 using the crystallographic data of Gatta et al. (2013). Hence, the above summarized approach
271 as used in this work to interpret the observed temperature variation of ΔE_Q, essentially
272 concerns a point-charge calculation of the ^5D level scheme.

273 In the case Fe^{2+}, the valence contribution to V_{ij} is restricted to the contribution of only
274 one of the six valence electrons and is thus given by:

275
$$V_{ij,val} = -e \frac{3x_i x_j - r^2 \delta_{ij}}{r^5} \quad (5)$$

Because the position of that one valence electron is not known, the expectation value ($<\hat{V}_{ij,val}>_p$) of the Stevens' equivalent operator representation $\hat{V}_{ij,val}$ for each ^5D level is calculated from the expression:

$$\hat{V}_{ij,val} = \frac{2}{21} e < r^{-3} > \left(\frac{3}{2} \left(\hat{L}_i \hat{L}_j + \hat{L}_j \hat{L}_i \right) - L(L+1)\hat{\delta}_{ij} \right), \quad (6)$$

$\hat{L}_i$ and $\hat{\delta}_{ij}$ being the equivalent operator expressions for the i-axis ($i = x, y, z$) component of the orbital moment (L) and the Kronecker delta, respectively. The quantity $< r^{-3} >$ is the expectation value related to the radial part of the ^5D wave functions. In this context, it should be noted that in the principal EFG-axes system, the relevant parameters can be expressed directly in Stevens' equivalent operators:

$$\hat{V}_{zz,val} = \frac{2}{21} e < r^{-3} > \left(3\hat{L}_z^2 - L(L+1)\hat{\delta}_{zz} \right) = \frac{2}{21} e < r^{-3} > \hat{O}_{20} \quad (7a)$$

$$\hat{V}_{xx,val} - \hat{V}_{yy,val} = \frac{2}{21} e < r^{-3} > \left(3\hat{L}_x^2 - 3\hat{L}_y^2 \right) = \frac{2}{7} e < r^{-3} > \hat{O}_{22}^c \quad (7b)$$

The superscript c in Equation 7b refers to the related cosine tesseral harmonic. The valence contribution to an EFG matrix component $V_{ij,val}$ at a given temperature T is subsequently obtained from the Boltzmann average of the expectation values for the operator expressions over the various ^5D orbital energy levels:

$$V_{ij,val} = \frac{\sum_p < \hat{V}_{ij,val} >_p \exp(-E_p / k_B T)}{\sum_p \exp(-E_p / k_B T)} \quad (8)$$

in which E_p and k_B are the energy of the p^{th} ($p = 1, 2, \ldots 5$) level and the Boltzmann constant, respectively.

In Fe^{2+} minerals (Fe^{2+} in the high spin state), the energy splitting between the higher E_g levels and the lower T_{2g} levels is usually so large that the valence contribution of these E_g levels to the quadrupole splitting at laboratory temperatures can be neglected (Ingalls 1964).

297 Therefore the valence contributions to the quadrupole splitting are in practice almost fully
298 determined by the Boltzmann occupation of the lower three orbital T_{2g} levels.

299 Finally, the lattice contribution to V_{ij} was calculated by a lattice summation over all
300 ions in the lattice, which are considered as point charges:

301 $$V_{ij,latt} = \sum_p eZ_p \frac{3x_{pi}x_{pj} - r_p^2\delta_{ij}}{r_p^5} \quad (9)$$

302 For the calculation of this lattice term, the center of the axes frame is chosen at the Mössbauer
303 nucleus. The quantity eZ_p in Equation 9 is the charge of the p^{th} ion, which is located at a
304 distance r_p of the Mössbauer probe and x_{pi} (i = 1,2,3) stands for the respective coordinates of
305 the p^{th} ion with respect to the Mössbauer probe.

306 In working out Equation 9 for the calculation of the lattice contribution, a coefficient
307 C_{lat} appears in the mathematical expression, *i.e.*,

308 $$C_{lat} = \tfrac{1}{2}e^2Q(1-\gamma_\infty)\,. \quad (10)$$

309 Using γ_∞ = -10.97 (Sternheimer 1972, Lauer et al. 1979), its value is calculated to be C_{lat} =
310 0.0027 nm^3 mm/s. In the initial fitting attempts C_{lat} was constraint to that value.

311 Further, because of the lack of data, *e.g.*, from optical spectroscopy, concerning the
312 positions of the upper E_g-levels in eosphorite, in the approach by the present authors the
313 expectation value $< r^4 >$ appearing in Eqation 4 was constrained to its theoretical value of
314 14.0 a.u. (Zhao and Du 1983). Note that 1 a.u. referring to a length dimension equals 5.29×10^{-11}m.

316 By fitting the as-developed theoretical model to the experimental $\Delta E_Q(T)$ curve for the
317 present eosphorite sample, two parameters were adjusted, *i.e.*, the expectation value $< r^2 >$
318 and a coefficient ΔE_0. This latter coefficient is a proportionality factor that is commonly used
319 in EFG calculations and that arises from the practice of expressing the valence contributions

to the EFG-components in units $\frac{4}{7}e<r^{-3}>$. In that respect, ΔE_0 can be considered as the free-ion zero-Kelvin axial valence term and is given by:

$$\Delta E_0 = \frac{2}{7}e^2Q(1-R)<r^{-3}>. \quad (11)$$

Values for the various constants appearing in Equation 11 have previously been calculated from theoretical models and can be found in literature: Q = 0.15 barn (Lauer et al. 1979), $<r^{-3}>$ = 4.93 a.u. (Freeman and Watson 1963), R = 0.12 (Sternheimer 1972, Lauer et al. 1979). With these theoretical values, ΔE_0 = 3.76 mm/s is calculated for the free-ion value. In real cases, however, ΔE_0 can be (strongly) reduced from this value due to covalence effects. Hence, ΔE_0 was considered as a parameter to be adjusted to the experimental $\Delta E_Q(T)$ curve.

The values of $<r^2>$ and ΔE_0 for the eosphorite sample were thus calculated to be 0.21 ± 0.02 a.u. and 1.48 ± 0.05 mm/s, respectively, giving the positions of the lower orbital levels relative to the ground state, Δ_1 and Δ_2, respectively (Table 2). The dotted line in Figure 7 represents the corresponding theoretical $\Delta E_Q(T)$ curve. The asymmetry parameter η was calculated to be 0.49 ± 0.05 at 4.2 K and 0.58 ± 0.05 at 250 K. These values are in reasonable agreement with the η values derived from the magnetic spectra and from the external-field spectrum obtained at 250 K (Table 1.) However, the sign of V_{zz} turned out to be positive, which is obviously in contrast with the negative sign found experimentally. Moreover, as Figure 7 shows, there are significant misfits between the theoretical $\Delta E_Q(T)$ curve and the observed values.

Searching for a possible reason for the disagreement between experimental and calculated results concerning the sign of V_{zz}, the influence of the OH^- and the H_2O groups located at the O4-ligand positions in the local Fe^{2+}-coordination of eosphorite was

342 investigated. It was determined that the charge distribution at these O4-positions drastically
343 affects the asymmetry parameter η and the sign of V_{zz}.

344 Bearing in mind that the EFG characteristics sensitively reflect the local coordination
345 of the Fe^{2+} site and that the refinement of the structural data as reported by Gatta et al. (2013)
346 concerned an eosphorite specimen with only a minor Fe^{2+} substitution at the Mn^{2+} sites, it is
347 suggested that the positions of the centers of charge of the Fe^{2+} coordination ligands for the
348 present eosphorite species most likely differ from those refined for the Mn-rich eosphorite. In
349 the latter case, the results of the structure-refinement calculations are indeed predominantly
350 determined by the Mn^{2+} coordination ligands, the presence of a small fraction of Fe^{2+}
351 coordination ligands being of minor importance. It is thought that such a difference for Fe^{2+}
352 with respect to Mn^{2+} can be taken into account in the crystal field calculation by introducing
353 an effective charge at the positions indicated by the structural data for Mn-rich eosphorite,
354 where the value is different from the expected ones on the basis of the chemical formula.
355 Assuming that the effective charges at the two O4 corners of the Mn octahedra are different,
356 *i.e.*, -1.0×e for O in H_2O (Z_{O4} = -1.0) and -1.5×e for O in OH^- (Z_{O4} = -1.5), results in a
357 negative sign for the calculated V_{zz}, in agreement with the experimental findings. The
358 parameters ΔE_0 and $\langle r^2 \rangle$ were adjusted to be 2.05 ± 0.05 mm/s and 0.09 ± 0.02 a.u.,
359 respectively. The as-such calculated values for the asymmetry parameter η and for the various
360 energy splittings Δ_i of the ^5D level scheme are indicated in Table 2. The corresponding
361 theoretical $\Delta E_Q(T)$ curve is plotted in Figure 7 as the dashed line, and it is obvious that, as
362 compared to the results obtained using charges of -2×e (Z_{O4} = -2.0) for both O4 ligands, better
363 agreement between calculated and experimental $\Delta E_Q(T)$ values is established.

364 Finally, an even more adequate description of the observed $\Delta E_Q(T)$ curve was obtained
365 by additionally considering the quantity C_{lat} as an adjustable parameter in the iteration. As
366 such, its value was found to be 3.1 ± 0.2 $\times 10^{-3}$ nm^3mm/s, which is reasonably close to the

theoretical value of 2.7×10^{-3} nm^3mm/s as obtained from Equation 10. The values for the other relevant quantities occurring in the model are included in Table 2. The solid line in Figure 7 represents the calculated $\Delta E_Q(T)$ variation, showing excellent agreement with the experimental results.

The strong reduction of the values for ΔE_0 and $\langle r^2 \rangle$ in comparison with the free ion values indicate a strong covalence of the Fe-O bonds, a phenomenon that inherently cannot be accurately taken into account by a point-charge calculation. The misfits of the calculated $\Delta E_Q(T)$ curve that exist at low temperatures may be due to neglecting the spin-orbit interaction that lifts the five-fold spin degeneracy of the orbital singlet states in the applied crystal field model. Depending on the strength of this interaction with respect to the level splittings (Δ_1 and Δ_2), it may cause $\Delta E_Q(T)$ to reach a shallow maximum at a certain low temperature, followed by a slight decrease on lowering the temperature, and subsequently by a slight increase on further lowering the temperature. This effect is clearly demonstrated by the simulations reported by Ingalls (1964) for a rhombic distortion. The relatively large energy difference (Δ_2 - Δ_1) between the lower ^5D orbital levels is consistent with the fact that the Fe octahedron in the eosphorite structure exhibits a strong distortion from axial symmetry. The present model calculations have shown that the asymmetry of the local EFG is strongly affected by the presence of an OH^- group and a H_2O molecule at the O4 corners of the local octahedral environment of the Fe^{2+} cation.

IMPLICATIONS

This study illustrates that ^{57}Fe Mössbauer spectroscopy, combined with proper analyzing procedures and model calculations for interpreting the results, can provide valuable structural and electronic information about the iron coordination polyhedra in minerals in general. If in addition the studied species orders magnetically, unique data concerning the

magnetic structure can be derived from the spectra. These conclusions explain why Fe-bearing minerals, including extraterrestrial ones, have formed, and undoubtedly will continue to form an important group of materials dealt with in the Mössbauer literature. This is especially true where it concerns oxides and silicates. For practical reasons, e.g. rareness and/or difficulties in collecting pure species in sufficient amounts for the experiments, Fe-bearing phosphates have less frequently received attention in mentioned literature. In recent years, the present research team has reported extensive Mössbauer studies of a number of different iron phosphates (Van Alboom et al. 2011; De Grave et al. 2013; Van Alboom and De Grave 2013) and it is the intention of the team to consider in the future several other phosphate species.

Eosphorite and childrenite are minerals formed by alteration of triphylite and lithiophilite, respectively. In pegmatites containing the latter two minerals, the Fe/Mn ratio is correlated to magmatic differentiation, in which higher Mn means more differentiation. Therefore, a thorough spectroscopic characterization of this type of minerals, especially at low temperatures at which magnetic ordering is established, can give information about the alteration of triphylite-lithiophilite into eosphorite-childrenite, indicating an oxidizing (presence of Fe^{3+}) or reducing (Fe^{2+}) environment. The presence of Fe^{3+} could also indicate a hydrothermal system with influence of meteoric water, whereas the presence of Fe^{2+} only could be related to the volatile products of the pegmatite differentiation.

In general, phosphate minerals play an important role in industrial activities such as the production of fertilizers and food processing. In the last decade, the interest of researchers in specifically Fe-containing phosphates has boomed tremendously as the result of the potential application of some of these materials to the development of practically useful rechargeable Li-ion batteries. Mössbauer spectroscopy for this application is an important experimental technique, in particular for measuring Fe^{2+}/Fe^{3+} ratios accurately during the

417 charging/discharging process and as such for the determination of the performance of the
418 involved batteries.

419 Also for many mineralogists, phosphate minerals are objects of interest for their broad
420 array of crystal structures and as indicators of rock paragenesis, particularly in the context of
421 planetary explorations. Although there are ample indications, for instance gathered by the
422 various instruments (including a miniature Mössbauer spectrometer called MIMOS) carried
423 by the Mars Exploration Rovers, so far the presence of phosphate minerals on various
424 locations on the planet has not yet been proven unambiguously. One reason is that the
425 Mössbauer parameters of Fe phosphates at ambient temperatures fall within the range of those
426 of other more abundant iron phases such as silicates and sulfates and can therefore not be
427 distinguished from these other phases. Eosphorite is a rare mineral on Earth, and probably
428 also on Mars. Nevertheless, investigations of the properties of this and other phosphate
429 minerals in general can indirectly help to identify phosphate minerals at the Martian surface.
430 Knowledge of the various properties these minerals will provide critical information about the
431 diverse environments in which they are formed and will so contribute to understand the actual
432 genesis of the Mars surface and the natural history of Mars in general.
433
434
435 **ACKNOWLEDGMENTS**

436 This work was partially funded by the Fund for Scientific Research – Flanders, and by
437 the Special Research Fund, UGent, Belgium. The authors are grateful to Dr. Ricardo Scholz for
438 kindly providing the sample and to Dr. M.D. Dyar for having composed the graph of Figure 1.
439
440

REFERENCES CITED

Blume, M., and Tjon, J.A. (1968) Mössbauer spectra in a fluctuating environment. Physical Review, 165, 446-461.

da Costa, G.M., Scholz, R., Karfunkel, J., Bermanec, V., and Chaves, M.L.S.C. (2005) ^{57}Fe-Mössbauer spectroscopy on natural eosphorite-childrenite-ernstite samples. Physics and Chemistry of Minerals, 31, 714-720.

De Grave, E. (1986) ^{57}Fe Mössbauer effect in ankerite: study of the electronic relaxation. Solid State Communication, 60, 541-544.

De Grave, E., and Van Alboom, A. (1991) Evaluation of ferrous and ferric Mössbauer fractions. Physics and Chemistry of Minerals, 18, 337-342.

De Grave, E., da Costa, G.M., Van Alboom, A., and Vandenberghe, R.E. (2013) Low-temperature Mössbauer study of heterosite, (Fe,Mn)PO_4. Spectrochimica Acta A, 100, 104-108.

Dyar, M.D., Jawin, E.R., Breves, E., Marchand, G., Nelms, M., Lane, M.D., Mertzman, S.A., Bish, D.L., and Bishop, J.L. (2014) Mössbauer parameters of iron in phosphate minerals: Implications for interpretation of martian data. American Mineralogist, 99, 914-942.

Eeckhout, S.G., and De Grave, E. (2003a) Evaluation of ferrous and ferric Mössbauer fractions: Part II. Physics and Chemistry of Minerals, 30, 142-146.

Eeckhout, S.G., and De Grave, E. (2003b) Fe-57 Mossbauer-effect studies of Ca-rich, Fe-bearing clinopyroxenes: Part I. Paramagnetic spectra of magnesian hedenbergite. American Mineralogist, 88, 1129-1137.

Freeman, A.J. and Watson, R.E. (1963) Antishielding of magnetic and electric hyperfine interactions in open shell ions. Physical Review, 131, 2566-2573.

Gatta, G.D., Nénert G., and Vignola P. (2013) Coexisting hydroxyl groups and H_20 molecules in minerals: A single-crystal neutron diffraction study of eosphorite, $MnAlPO_4(OH)_2.H_2O$. American Mineralogist, 98, 1297-1301.

Hanson, A.W. (1960) The crystal structure of eosphorite. Acta Crystallographica, 13, 384-387.

Hoyos, M.A., Calderon, T., Vergara, I., and Garcia-Solé, J. (1993) New structural and spectroscopic data for eosphorite. Mineralogical Magazine, 57, 329-336.

Hoy, G.R., and Chandra, S. (1967) Effective Field Parameters in Iron Mössbauer Spectroscopy. Journal of Chemical Physics, 47, 961-965.

Huminicki, D.M.C., and Hawthorne, F.C. (2002) The crystal chemistry of the phosphate minerals. In M.J. Kohn, J. Rakovan and J.M. Hughes, Eds, Phosphates, vol. 48, p.123-253. Reviews in Mineralogy and Geochemistry, Mineralogical Society of America, Washington DC.

Hutchings, M.T. (1964) Point-charge calculations of energy levels of magnetic ions in crystalline electric fields. Solid State Physics, 16, 227-273.

Ingalls, R. (1964) Electric-field gradient tensor in ferrous compounds. Physical Review, 133, 787-795.

Kündig, W. (1967) Evaluation of Mössbauer spectra for ^{57}Fe. Nuclear Instruments and Methods in Physics Research, 48, 219-228.

Lauer, S., Marathe, V.R., Trautwein, A. (1979) Sternheimer shielding using various approximations. Physical Review A, 19, 1852-1861.

Perkins, H.K. and Hazony, Y. (1972) Temperature-dependent crystal field and charge density: Mossbauer studies of FeF_2, $KFeF_3$, $FeCl_2$, and FeF_3. Physical Review B, 7-18.

Sternheimer, R. M. (1972) Quadrupole shielding and antishielding factors for several atomic ground states. Physical Review A, 6, 1702-1709.

Van Alboom,A., and De Grave, E. (2013) Relaxation effects and re-entrent spin glass behavior at low temperatures in natural strunzite, ferristrunzite and ferrostrunzite. American Mineralogist, 98, 1497-1507.

Van Alboom, A., De Grave, E., and Wohlfahrt-Mehrens, M. (2011) Temperature dependence of the Fe^{2+} Mössbauer parameters in triphylite ($LiFePO_4$). American Mineralogist, 96, 408-416

Vandenberghe, R.E., De Grave, E., and de Bakker, P.M.A. (1994) On the methodology of the analysis of Mössbauer spectra. Hyperfine Interactions, 83, 29-49.

Varret, F. (1976) Mössbauer spectra of paramagnetic powders under applied field: Fe^{2+} in fluosilicates. Journal of Physics and Chemistry of Solids, 37, 265-271.

Zhao, M., and Du, M. (1983) Two-center transitions in the antiferromagnetic salt $FeCO_3$. Physical Review B, 28, 6481-6484.

Figure captions

Figure 1. Polyhedral representation of the orthorhombic structure of eosphorite, showing the chains of distorted Mn and more regular Al octahedra. All the iron in the eosphorite structure is localized at the Mn sites, because both ions have nearly the same dimensions and the same valence state. Red: O; yellow: H; green tetrahedron: P site; pink octahedron: Mn site; blue octahedron: Al site.

Figure 2. Experimental and calculated (solid line) Mössbauer spectrum of the eosphorite sample at 295 K. The size of the symbols (+) roughly corresponds to twice the standard deviation (2σ) of the experimental counts.

Figure 3. Experimental and calculated (solid line) Mössbauer spectrum of the eosphorite sample at 250 K in a longitudinal external magnetic field of 60 kOe. The size of the symbols (+) roughly corresponds to twice the standard deviation (2σ) of the experimental counts.

Figure 4. Experimental and calculated (solid line) Mössbauer spectrum of the eosphorite sample at 4.2 K. The size of the symbols (+) roughly corresponds to twice the standard deviation (2σ) of the experimental counts.

Figure 5. Mössbauer spectra of eosphorite at (a) 19 K and (b) 10 K. The spectra have been fitted with a superposition of a slow and a fast relaxation component (solid lines). The size of the symbols (+) roughly corresponds to twice the standard deviation (2σ) of the experimental counts.

Figure 6. Isomer shift (δ) plotted as a function of temperature. The solid line is the calculated temperature dependence on the basis of the Debye approximation for the lattice vibrations.

Figure 7. Temperature dependence of the quadrupole splitting ΔE_Q of Fe^{2+} in eosphorite. The lines represent the theoretical curves calculated from the crystal field model

for the real symmetry of the Fe^{2+} site in eosphorite (Gatta et al. 2013). **a** (wine dash-dot line): Z_{O4} = -2.0, C_{lat} = 2.7×10^{-3} nm^3mm/s (fixed); **b** (blue dashed line): Z_{O4} = -1.0 and -1.5, C_{lat} = 2.7×10^{-3} nm^3mm/s (fixed); **c** (red solid line): Z_{O4} = -1.0 and -1.5, C_{lat} = 3.1×10^{-3} nm^3mm/s (adjusted). Corresponding values of calculated relevant quantities are given in Table 2.

Table 1. Adjusted values for the isomer shift δ_{Fe}, the quadrupole spitting ΔE_Q and the EFG asymmetry parameter η of eosphorite at selected temperatures. Numbers within parentheses give an indication of the error on the corresponding parameter values.

T (K)	δ_{Fe} (mm/s)	ΔE_Q (mm/s)	V_{zz}	H
4.2	1.37(1)	2.15(2)	< 0	0.51(5)
10	1.38(1)	2.17(2)		0.50(5)
19	1.38(1)	2.21(2)		0.58(5)
40	1.380(4)	2.148(5)		
80	1.366(4)	2.149(5)		
140	1.334(4)	2.033(5)		
200	1.298(4)	1.892(5)		
250‡	1.25(2)	1.88(3)	< 0	0.45(5)
260	1.261(4)	1.789(5)		

‡: MS recorded in an external magnetic field H_{ext} of 60 kOe

Table 2. Results concerning the quadrupole splitting calculations using the point-charge model within the crystal field approximation. Z_{O4} is the "charge number" (times the proton charge) of the O4-ligands of the Fe^{2+} coordination in eosphorite (there are two O4 ligands; following Gatta et al. 2013: the one is H_2O and the other is OH^-). Δ_i (i = 1,…,4) is the position of the i^{th} orbital level in the ^5D level scheme of Fe^{2+}relative to the ^5D orbital ground level. For the other symbols: see text.

$\|Z_{O4}\|$ (H_2O)	$\|Z_{O4}\|$ (OH^-)	ΔE_0 (mm/s)	$\langle r^2 \rangle$ (a.u.)	C_{lat}*	V_{zz}	Δ_1 (cm^{-1})	Δ_2 (cm^{-1})	Δ_3 (cm^{-1})	Δ_4 (cm^{-1})	η (4.2K)	η (250K)
2.0	2.0	1.48	0.21	2.7	>0	320	570	7130	7320	0.49	0.58
1.0	1.5	2.05	0.09	2.7	<0	300	1020	6030	6870	0.84	0.54
1.0	1.5	2.02	0.11	3.1	<0	280	970	6000	6870	0.79	0.46

* in units $10^{-3}(nm)^3 mm/s$

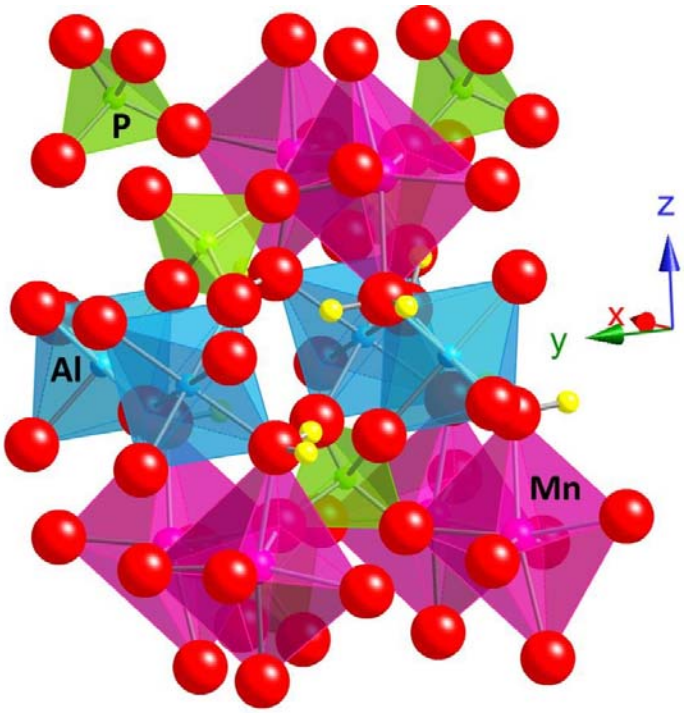

Figure 1

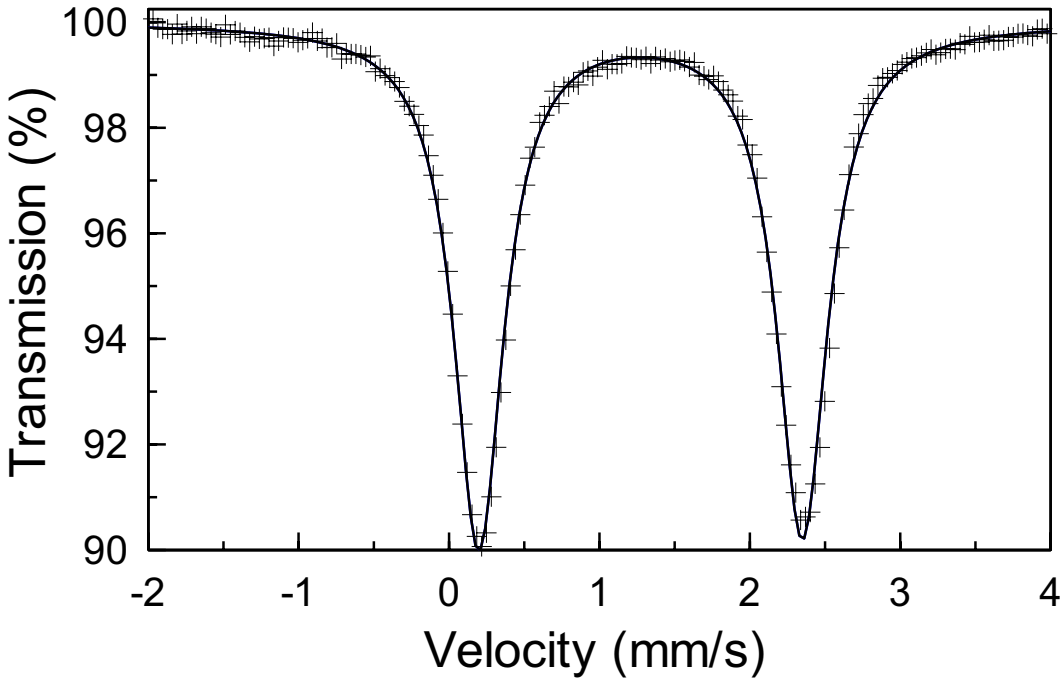

Figure 2

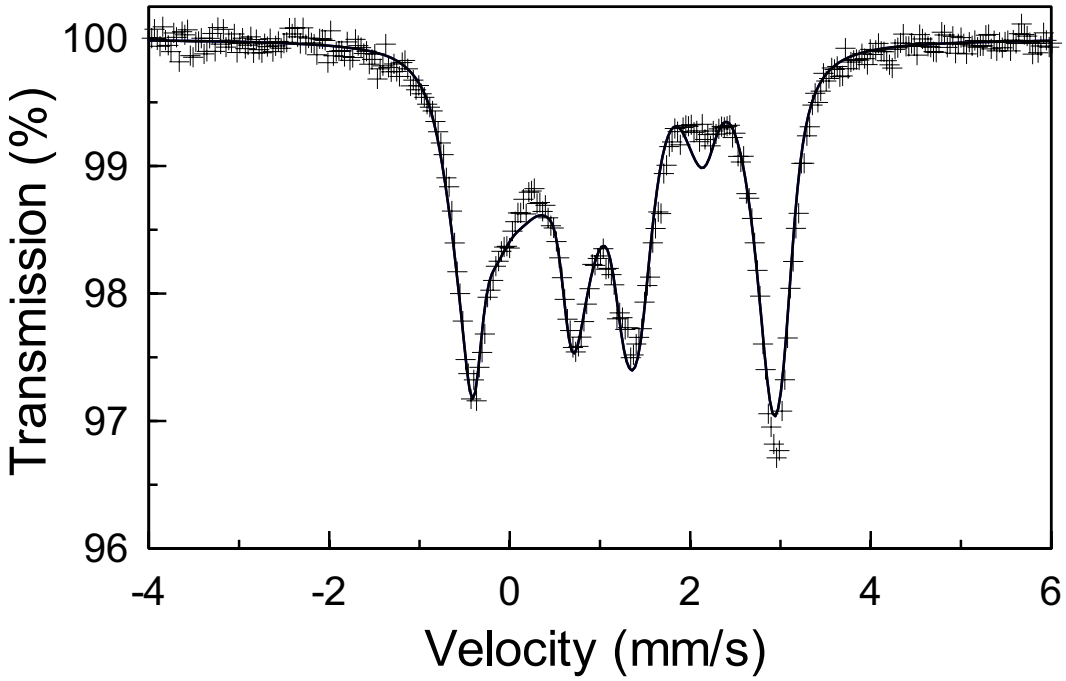

Figure 3

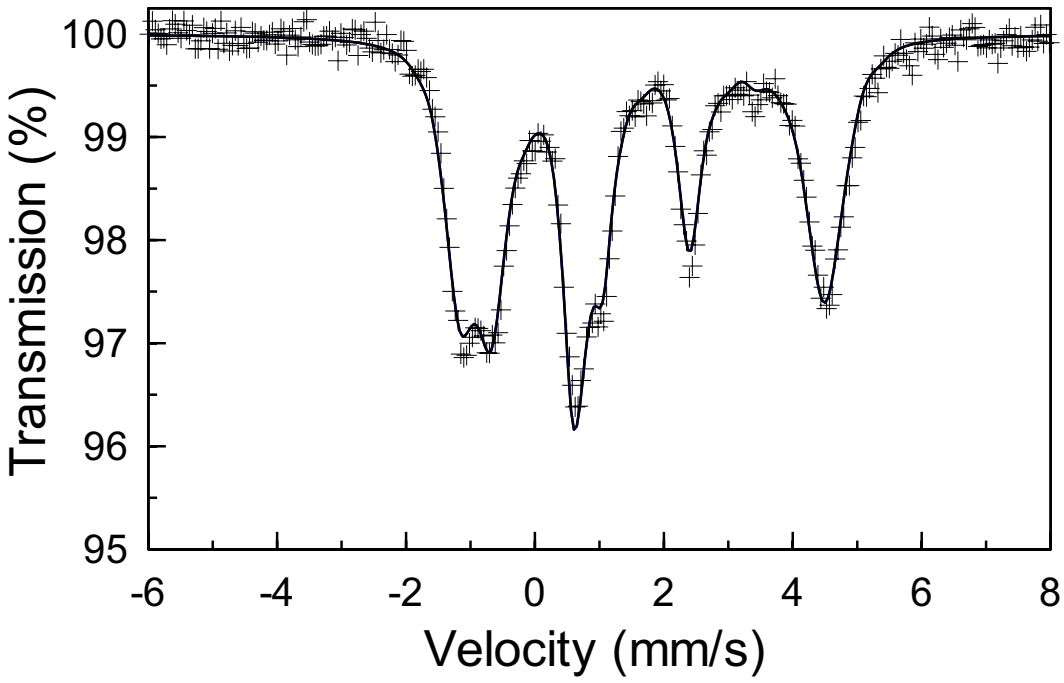

Figure 4

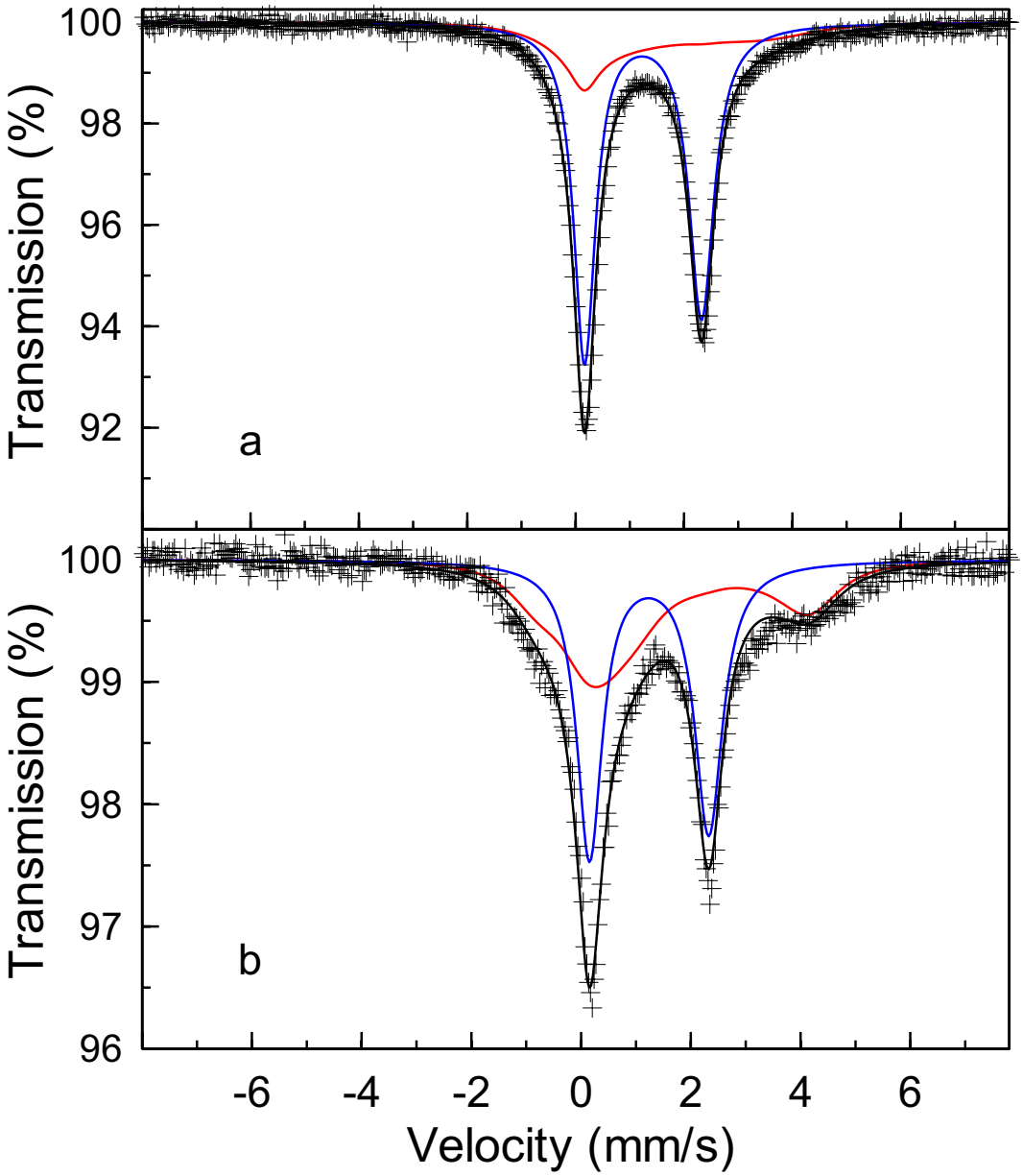
Transmission (%)
100
98
96
94
92
a
Transmission (%)
100
99
98
97
96
b
-6
-4
-2
0
2
4
6
Velocity (mm/s)

Figure 5

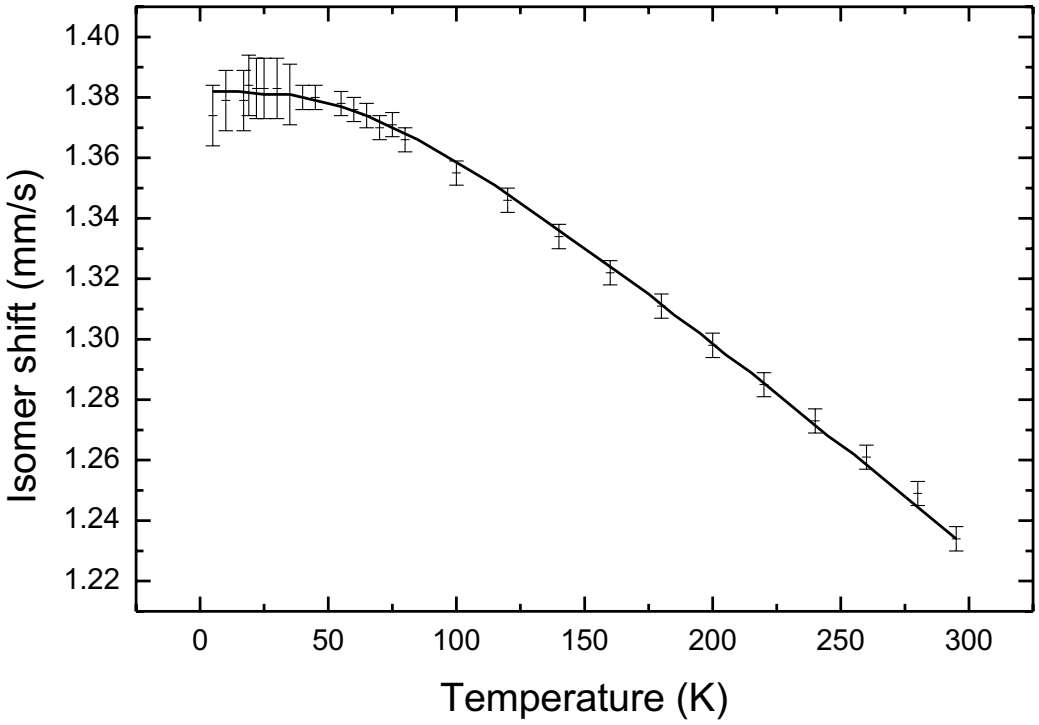
Isomer shift (mm/s)
1.40
1.38
1.36
1.34
1.32
1.30
1.28
1.26
1.24
1.22
0
50
100
150
200
250
300
Temperature (K)

Figure 6

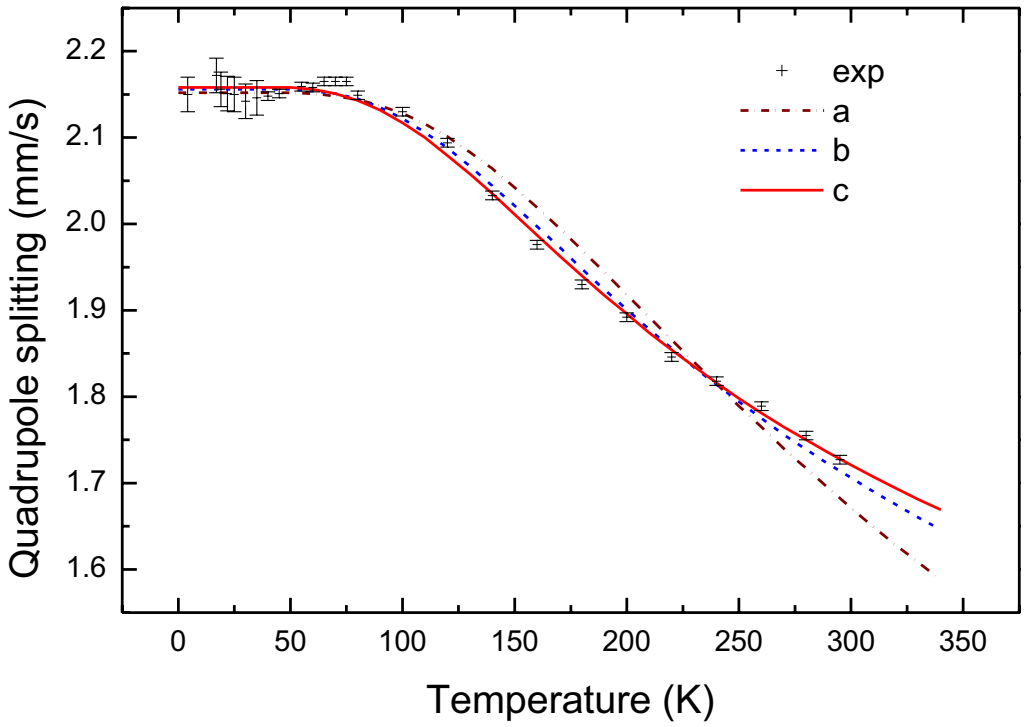
Quadrupole splitting (mm/s)
Temperature (K)
exp
a
b
c
2.2
2.1
2.0
1.9
1.8
1.7
1.6
0
50
100
150
200
250
300
350

Figure 7